SUPPORTING INFORMATION

Chemically Tunable Full Spectrum Optical Properties of 2D Silicon Telluride Nanoplates

Mengjing Wang[†,‡], *Gabriella Lahti*[†], *David Williams*[†], *and Kristie J. Koski*[†*]

†Department of Chemistry, University of California Davis, Davis California 95616, USA
‡ Department of Chemistry, Brown University, Providence Rhode Island 02912, USA
* koski@ucdavis.edu

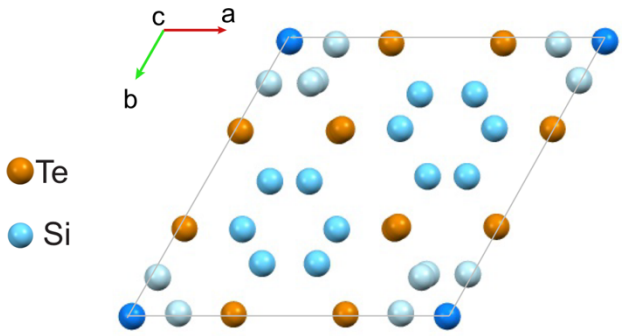

Fig S1. Structure of the silicon telluride unit cell viewed from the top-down in projection showing possible partial occupancies of the silicon atoms. Si_2Te_3 has four possible equivalent positions of the Si-Si or substitutional Si-Ge dumbbells. Dopant germanium can take the place of any of the silicon atoms, and all replacements are equally likely.

$Si_{2-x}Ge_xTe_3$	X = 0	X = 0.04	X = 0.10	X = 0.12	X = 0.22
E_g (cm^{-1})	98.2 +/- 0.8	99.6 +/- 1.6	101.6 +/- 1.9	102.6 +/- 1.4	102.9 +/- 1.0
$A^1{}_{1g}$(cm^{-1})	127.0 +/- 0.4	126.6 +/- 2.0	127.1 +/- 0.3	127.2 +/- 0.8	126.6 +/- 0.5
$A^2{}_{1g}$(cm^{-1})	143.9 +/- 0.2	143.4 +/- 0.1	143.5 +/- 0.3	143.1 +/- 0.3	143.2 +/- 0.2

Table S1. Raman frequency shifts of germanium-doped silicon telluride ($Si_{2-x}Ge_xTe_3$).

Intercalant	None	+ Cu	+ Ge
E_g (cm^{-1})	98.2 +/- 0.8	99.9 +/- 0.8	101.1 +/- 0.3
A^1_{1g}(cm^{-1})	127.0 +/- 0.4	122.0 +/- 0.5	126.4 +/- 0.6
A^2_{1g}(cm^{-1})	143.9 +/- 0.2	144.4 +/- 0.4	143.5 +/- 0.6

Table S2. Raman frequency shifts of silicon telluride intercalated with copper ($Cu_{0.18}Si_2Te_3$) and germanium ($Ge_{0.06}Si_2Te_3$).

$Si_{2-x}Ge_xTe_3$	a (Å)	c (Å)	Volume (Å ^{3})
Si_2Te_3	7.423 +/- 0.003	13.49 +/- 0.01	643.6 +/- 0.8
X = 0.04	7.428 +/- 0.001	13.45 +/- 0.01	642.6 +/- 0.5
X = 0.10	7.433 +/- 0.003	13.48 +/- 0.01	644.8 +/- 0.7
X = 0.12	7.438 +/- 0.005	13.47 +/- 0.02	645.4 +/- 1.2
X = 0.22	7.438 +/- 0.004	13.47 +/- 0.01	645.2 +/- 1.0

Table S3. Lattice constants and unit cell volume of germanium-doped Si_2Te_3 with varying amounts of germanium doping content, x. Lattice constants are determined through Rietveld Refinement using Maud.[1s]

Intercalant	a (Å)	c (Å)	Volume (Å ^{3})
None	7.423 +/- 0.003	13.49 +/- 0.01	643.6 +/- 0.8
Cu	7.430 +/- 0.001	13.49 +/- 0.01	644.99 +/- 0.3
Ge	7.417 +/- 0.003	13.48 +/- 0.01	642.3 +/- 0.6

Table S4. Lattice constants and unit cell volume of Si_2Te_3 along with intercalated with ~3 at% of copper and ~1 at % of germanium. Lattice constants are determined through Rietveld Refinement using Maud.[1s]

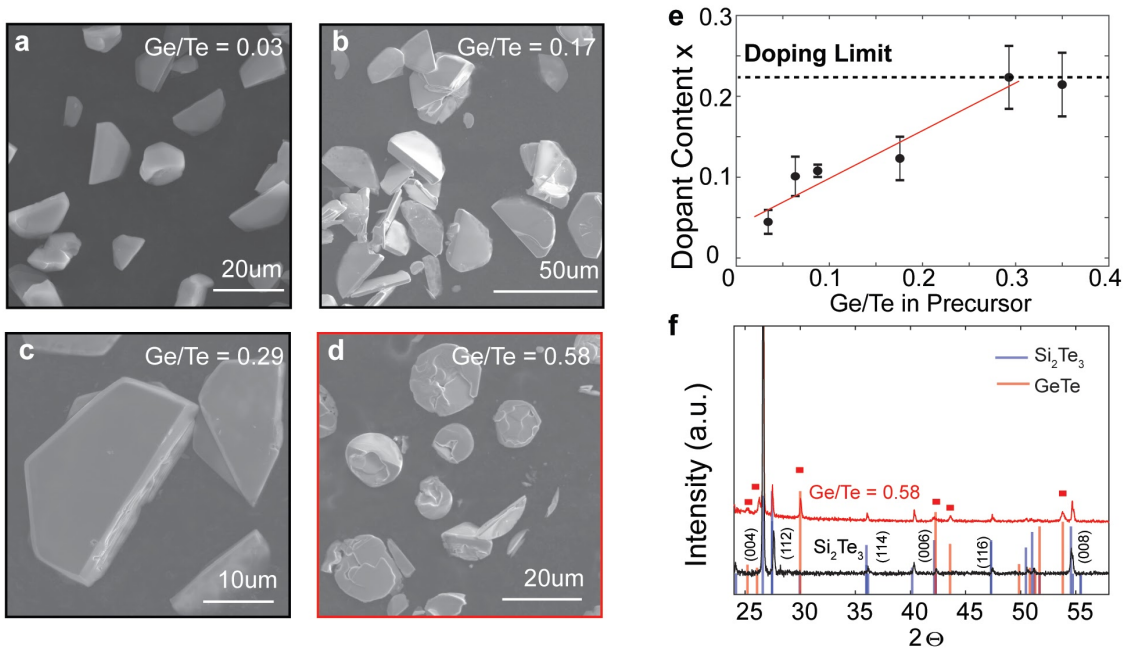

Fig S2. (a-c) SEM images of $Si_{2-x}Ge_xTe_3$ hexagonal plates standing upright on the substrate using different Ge/Te ratios in precursor are shown. (d) When Ge/Te ratio are greater than 0.29, such as Ge/Te = 0.58, phase separation occurs with formation of irregularly shaped crystals. (e) Germanium dopant content, x, is linear in relation with Ge/Te solid precursors below a nominal doping limit of x = 0.22 above which maximum saturation is reached. (f) Powder XRD of doped Si_2Te_3 using a Ge/Te ratio of 0.58 shows extra peaks (red squares) which belong to GeTe, indicating phase separation. Phase separation is expected beyond a specific germanium concentration from competing formation of germanium telluride and $Ge_{0.9}Si_{0.1}Te$ which has been noted in the alloy phase diagram from bulk growth processes.[2s]

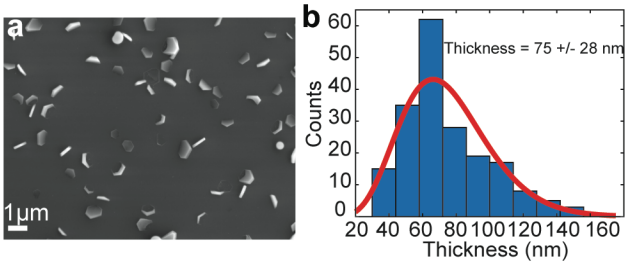

Fig S3. (a) Example scanning electron microscope (SEM) of $Si_{1.84}Ge_{0.16}Te$ nanoplates grown vertically on a silicon substrate with the van der Waals gap of many plates situated upright to easily measure the thickness

and thickness distribution. (b) The average thickness of the germanium doped silicon telluride is 75 +/- 28 nm ranging from 40 nm to 150 nm.

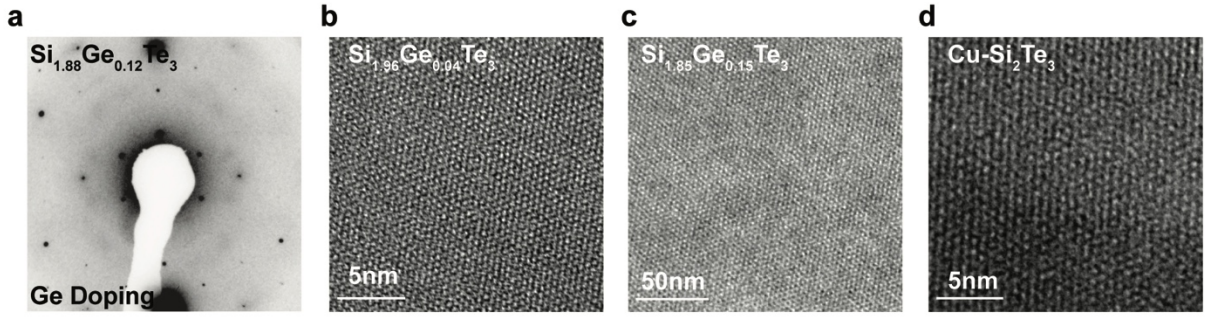

Fig S4. (a) Selected area electron diffraction (SAED) of germanium doped silicon telluride ($Si_{1.88}Ge_{0.12}Te_3$) along with high-resolution transmission electron microscope (TEM) images of (b) $Si_{1.96}Ge_{0.04}Te_3$, (c) $Si_{1.85}Ge_{0.15}Te_3$, and (d) 2 at.% copper-intercalated silicon telluride demonstrate that doping and intercalation maintain the crystallinity of the silicon telluride nanocrystals.

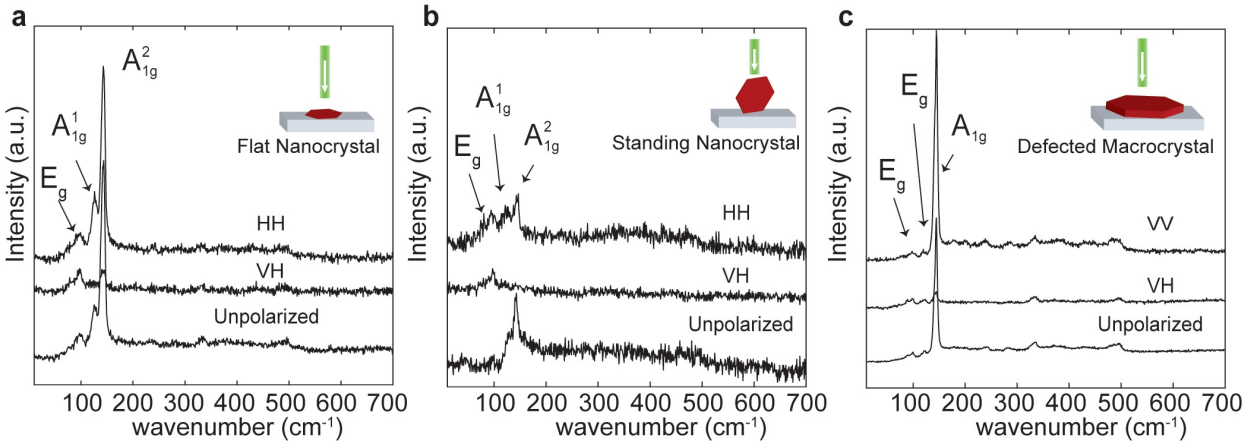

Fig S5. A concise analysis of the vibrational modes of silicon telluride has been made by Zwick *et al.*[3s] Given its point group, silicon telluride (point group D_{3d}) should also have Raman mode assignments similar to Bi_2Se_3 (point group D_{3d}).[4s] Raman scattering on nanoplates lying flat on a substrate and standing on a substrate were investigated using parallel configuration of the polarizations (VV, HH) and perpendicular configurations (VH, HV). In the perpendicular configuration of polarization, observation of the A_{1g} modes

should be eliminated.[3s,4s] (a) Raman scattering of a flat Si_2Te_3 nanoplate probed in a backscattering geometry with the *c*-axis perpendicular to the laser beam shows the A_{1g} modes vanish. Some of the remaining intense phonon peak at 147 cm^{-1} may be due to leakage from the sample not sitting completely flat on the surface or other excitation. (b) A standing silicon telluride nanocrystal measured in a backscattering geometry with the *c*-axis parallel to the incoming laser beam. The A_{1g} peaks vanish at cross-polarizer configurations. (c) A defected silicon telluride macrocrystal with assignment of A_{1g}, E_g modes similar to Zwick et al.[3s] This is a large defected crystal that does not show the additional A_{1g} mode.

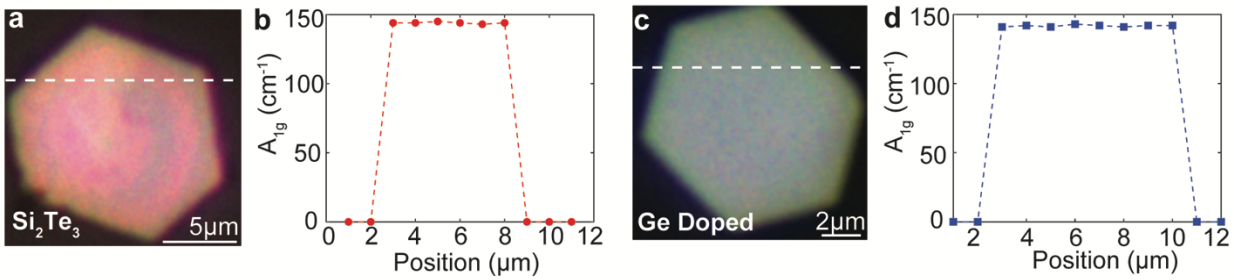

Fig S6. (a) One-dimensional Raman image of a Si_2Te_3 plate and a $Si_{1.84}Ge_{0.16}Te_3$ nanoplate showing the position of the A_{1g} mode. No change is seen in the sample at this resolution scale which suggests that doping is consistent throughout.

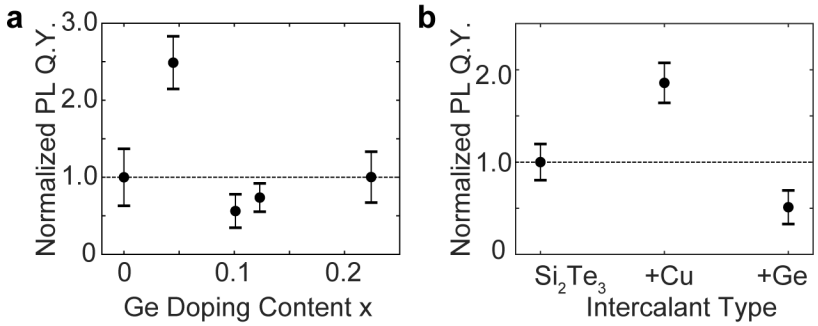

Fig S7. Normalized photoluminescence quantum yield of Ge doping in (a) shows about 2.5 times increase of quantum yield at x = 0.04, but remain unchanged beyond x = 0.04 within error. (b) Normalized PL quantum yield of Si_2Te_3 intercalated with ~ 3atm% copper shows a 1.9 times increase of quantum yield, while germanium intercalation shows a decrease of PL quantum yield.

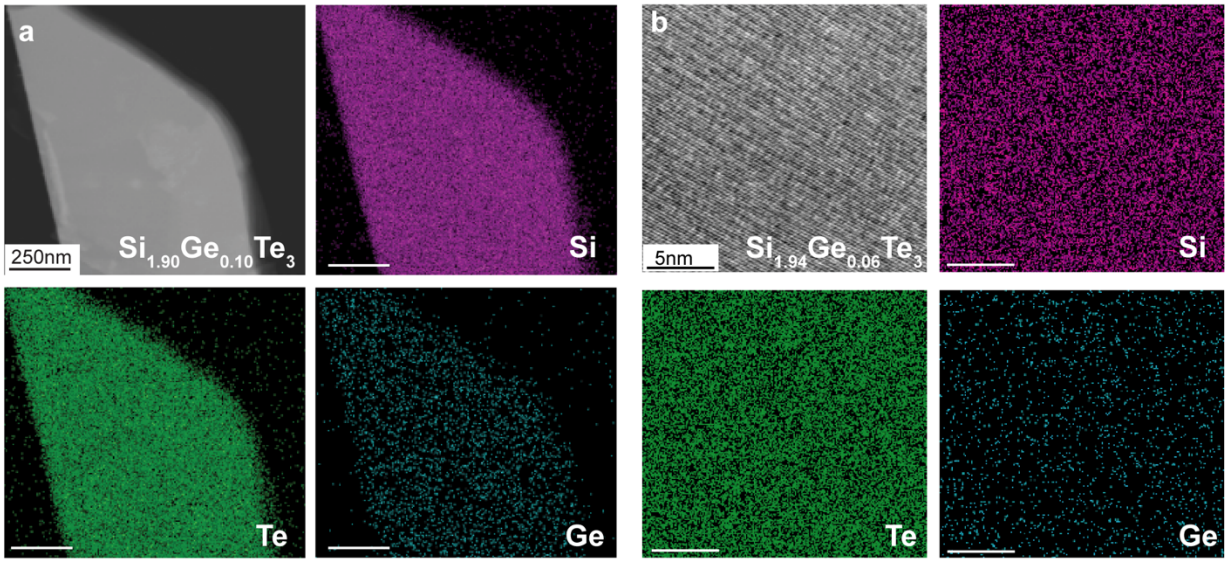

Fig S8. STEM-EDX elemental map of a germanium doped silicon telluride nanoplate ($Si_{2-x}Ge_xTe_3$) with (a) x = 0.10 and (b) x = 0.06.

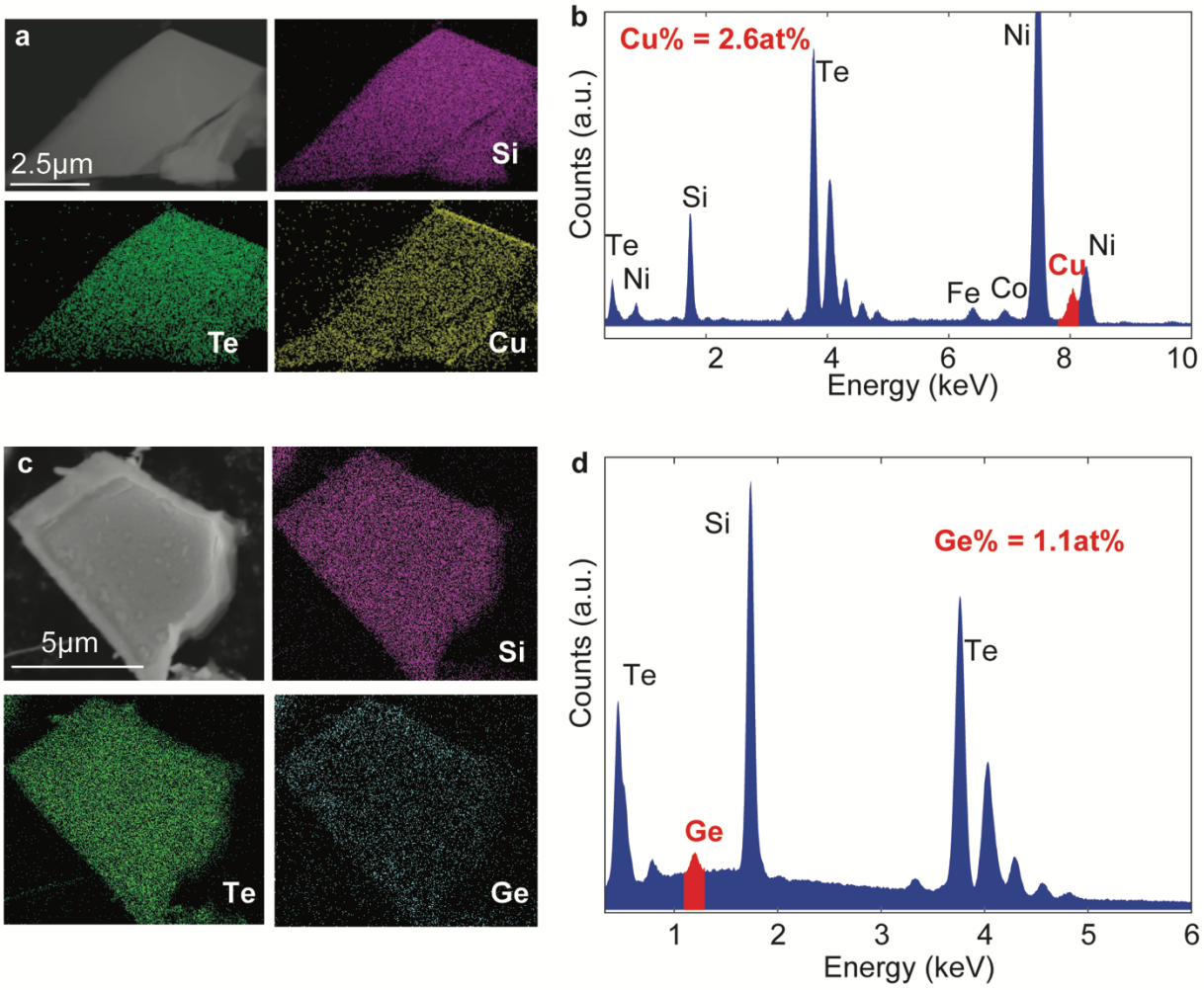

Fig S9. (a) STEM-EDX mapping of copper-intercalated silicon telluride, and (b) corresponding EDX spectrum shows that about 2.6 at.% of copper (red) was intercalated. Ni signal comes from the TEM grid, Fe and Co signals originate from the sample holder. (c) SEM-EDX mapping of silicon telluride plate intercalated with germanium, (d) corresponding EDX spectrum shows about 1.10 at% germanium (red) was intercalated.

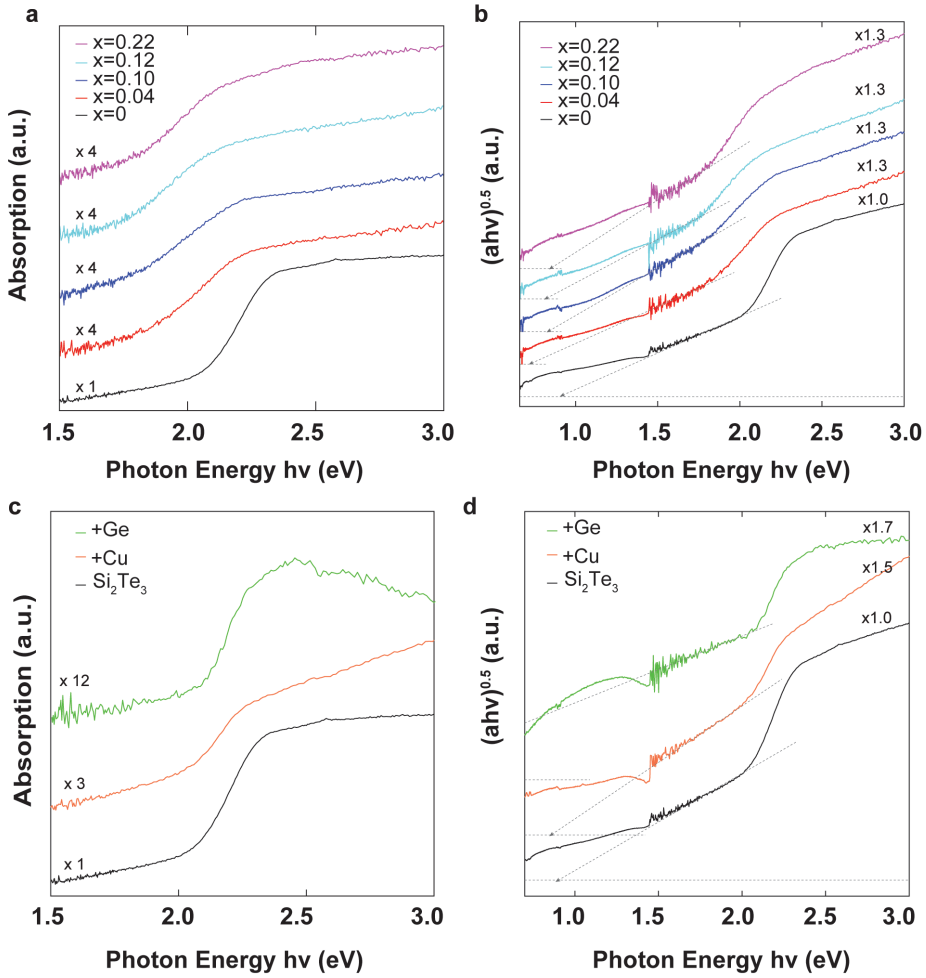

Fig S10. (a) UV-Vis absorption data of germanium-doped silicon telluride. The large noise and cut-off near the 1.5eV region is from the change of the UV-Vis detectors.(b) Indirect band gap energies were determined from a Tauc plot of $(ahv)^{0.5}$~hv. (c) UV-Vis absorption data of silicon telluride after intercalation of copper and germanium. (d) Indirect band gap energies were determined from a Tauc plot analysis of $(ahv)^{0.5}$~hv. The fit of $(ahv)^{0.5}$~hv for germanium intercalation has an intersection value that extrapolates to approximately 0 eV.

REFERENCES

[1s] Maud: Materials Analysis Using Diffraction, Version 2.79. http://maud.radiographema.eu (accessed Nov 5, 2017)

[2s] Babareko A. A.; Tsu Tsung T.; Savitskii E. M. Crystal Lattice Defects Produced during Deformation of Molybdenum and Molybdenum-Rhenium Alloy. *Russ. Metall. Min.* **1964**, *1*, 121-122.

[3s] Zwick, U.; Rieder, K.H. Infrared and Raman Study of Si_2Te_3. *Z. Phys. B: Condens. Matter* **1976**, *25*, 319-322.

[4s] Zhang, X.; Tan, Q. H.; Wu, J. B.; Shi, W.; Tan, P. H. Review on the Raman Spectroscopy of Different Types of Layered Materials. *Nanoscale*, **2016**, *8,* 6435-6450.